The influence of crustal recycling on the molybdenum isotope composition of the Earth's mantle

Remco C. Hin[1,2]*, Kate E.J. Hibbert[1], Shuo Chen[1,3,4], Matthias Willbold[1,5], Morten B. Andersen[1,6], Ekaterina S. Kiseeva[7,8], Bernard J. Wood[7], Yaoling Niu[9], Kenneth W.W. Sims[10], Tim Elliott[1]

[1]*School of Earth Sciences, University of Bristol, Bristol BS8 1RJ, UK*

[2]*Now at: Bayerisches Geoinstitut, Universität Bayreuth, 95447 Bayreuth, Germany*

[3]*Key Laboratory of Marine Geology and Environment, Institute of Oceanology, Chinese Academy of Sciences, Qingdao 266071, China.*

[4]*Laboratory for Marine Geology, Qingdao National Laboratory for Marine Science and Technology, Qingdao 266061, China*

[5]*Now at: Geowissenschaftliches Zentrum, Georg-August-Universität Göttingen, 37077 Göttingen, Germany*

[6]*Now at: School of Earth and Environmental Sciences, Cardiff University, Cardiff CF10 3AT, UK*

[7]*Department of Earth Sciences, University of Oxford, Oxford OX1 3AN, UK*

[8]*Now at: School of Biological, Earth and Environmental Sciences, University College Cork, Cork T23 N73K, Ireland*

[9]*Department of Earth Sciences, Durham University, Durham DH1 3LE, UK*

[10]*Department of Geology and Geophysics, University of Wyoming, Laramie, WY 82071, USA*

*Corresponding author: remco.hin@uni-bayreuth.de

Abstract

Several studies have suggested that the Earth's upper mantle is slightly enriched in light molybdenum isotopes relative to bulk Earth, defined by chondrites, but there is no consensus on the presence of this subtle but potentially notable signature. To establish better whether or not the $^{98}Mo/^{95}Mo$ of Earth's upper mantle is indeed sub-chondritic, we have analysed hand-picked glasses of depleted (i.e. chondrite normalised La/Sm<1) mid-ocean ridge basalts (MORB) from the Pacific, Atlantic and Indian ocean basins. The mean Mo isotope composition of our depleted MORB relative to reference NIST SRM 3134 ($\delta^{98/95}Mo_{NIST\ SRM\ 3134}$) is −0.22±0.03‰ (95% confidence interval, c.i.) compared to a value of −0.15±0.01‰ (95% c.i.) for bulk Earth. Our high precision analyses of the $^{234}U/^{238}U$ activity ratios of these samples are within uncertainty of unity, which rules out the effect of possible secondary, sea-floor processes as the dominant cause of their low $\delta^{98/95}Mo_{NIST\ SRM\ 3134}$. We further report experimental data showing that sulphide liquid has $\delta^{98/95}Mo_{NIST\ SRM\ 3134}$ 0.25±0.01‰ lower than basaltic silicate liquid at 1400°C. This fractionation is too small to significantly alter the Mo isotope composition of basalts relative to their sources during melting or differentiation.

Our MORB data show that resolvably sub-chondritic Mo isotope compositions are common in the upper mantle. Moreover, an appropriately weighted average $\delta^{98/95}Mo_{NIST\ SRM\ 3134}$ of depleted and enriched MORB, taken from this study and the literature, yields an estimated mantle value of −0.20±0.01‰, indicating that the upper mantle as a whole is sub-chondritic. Since prior work demonstrates that core formation will not create a residual silicate reservoir with a sub-chondritic $\delta^{98/95}Mo_{NIST\ SRM\ 3134}$, we propose that this feature is a result of recycling oceanic crust with low $\delta^{98/95}Mo_{NIST\ SRM\ 3134}$ because of Mo isotope fractionation during subduction dehydration. Such an origin is in keeping with the sub-chondritic Th/U and low Ce/Pb of the depleted mantle, features which cannot be explained by simple melt extraction. We present mass balance models of the plate tectonic cycle that quantitatively illustrate that the $\delta^{98/95}Mo_{NIST\ SRM\ 3134}$ of the Earth's mantle can be suitably lowered by such oceanic crustal recycling. Our Mo isotope study adds to the notion that the depleted mantle has been substantially modified by geodynamic cycling of subduction-processed oceanic crust.

1 Introduction

Traditionally, trace element abundances and radiogenic isotopes have been used to investigate the recycling of elements from crust to mantle and its consequences for the chemical evolution of the terrestrial mantle. Mass-dependent variations in isotope ratios have also attracted attention as proxies for this process, as relatively large isotopic fractionations at low temperatures near the Earth's surface should diagnostically fingerprint recycled material (e.g. Andersen et al., 2015). Molybdenum isotope measurements of mantle derived samples offer some promise in this context. Notably, fractionation during dehydration of the subducting slab appears to generate a fluid with isotopically heavy Mo, as inferred from the compositions of mafic arc lavas (Freymuth et al., 2015; König et al., 2016; Villalobos-Orchard et al., 2020), and a complementary, isotopically light residue, manifest in exhumed eclogites (Chen et al., 2019). Stirring subduction-processed material back into the mantle should therefore impart an isotopically light Mo signature (Chen et al., 2019; Freymuth et al., 2015), although a similar effect has been proposed to result from melt depletion (McCoy-West et al., 2019).

An attractive aspect of the Mo isotope system is that as a refractory and siderophile element, analyses of chondrites and (magmatic) iron meteorites should provide a reliable estimate for the bulk Earth, and a reference against which the effects of recycling can be gauged. Two studies of such meteorites yield consistent $\delta^{98/95}Mo_{NIST\ SRM\ 3134}$ (i.e. $^{98}Mo/^{95}Mo$ relative to international reference standard NIST SRM 3134; hereafter $\delta^{98/95}Mo$), with values of −0.16±0.02‰ (Burkhardt et al., 2014) and −0.14±0.01‰ (Liang et al., 2017), yielding an overall mean of −0.15±0.01‰. For simplicity, we henceforth refer to this value as 'chondritic'. Although Mo is siderophile, and so the Mo abundance of the silicate Earth is strongly influenced by core formation, experimental studies imply that metal segregation either does not fractionate the Mo isotope composition of the residual silicate mantle or slightly enriches it in heavy Mo isotopes (Hin et al., 2019, 2013). Thus, recent studies of (ultra-)mafic rocks suggesting that the Mo isotope composition of the Earth's mantle is isotopically light relative to chondrites (Bezard et al., 2016; Liang et al., 2017; McCoy-West et al., 2019), seemingly identify a significant geochemical perturbation of the mantle since core-mantle separation.

Agreement on the $\delta^{98/95}Mo$ of Earth's mantle, however, has not yet emerged. There appears a tendency of depleted MORB (i.e. with sub-chondritic La/Sm or $(La/Sm)_N<1$) to have sub-chondritic

79 $\delta^{98/95}$Mo and enriched MORB (i.e. $(La/Sm)_N$>1) to have slightly super-chondritic $\delta^{98/95}$Mo (Bezard et
80 al., 2016; Chen et al., 2022). Yet, the study by Bezard et al. (2016) also documents two depleted MORB
81 with positive $\delta^{98/95}$Mo, while Liang et al. (2017) obtained super-chondritic values for all their depleted
82 and enriched MORB. Given this uncertainty in the composition of the modern mantle, it is unsurprising
83 that there are also different perspectives on the evolution of $\delta^{98/95}$Mo through mantle history. A dataset
84 of bulk komatiite analyses, with highly variable $\delta^{98/95}$Mo, has been filtered for the effects of alteration
85 and used to argue for sub-chondritic mantle $\delta^{98/95}$Mo as early as the Archaean (McCoy-West et al.,
86 2019). Yet, previously, some of these same analyses were used to argue for a chondritic Archaean
87 mantle (Greber et al., 2015).
88 Our main aim here is to try to evaluate better the $\delta^{98/95}$Mo of the modern, upper mantle. To this
89 end, we analyse a new set of samples focussed on depleted MORB. To aid in interpretation, we also
90 present results from sulphide-silicate experiments to investigate the importance of fractionation
91 between these two phases in accounting for observed Mo isotope variability, as Mo isotope fractionation
92 might occur during removal of sulphide on both a local (sulphur fractionation during MORB genesis;
93 Mathez, 1976) and global scale (O'Neill, 1991).
94
95 **2 Samples**
96 All MORB analyses are made on fresh, hand-picked glasses from previously well-characterised
97 samples. We analysed samples from active spreading centres in the three major ocean basins. Five
98 samples are from the East Pacific Rise between 9°30'-11°30' N (Niu et al., 1999; Regelous et al., 1999;
99 Sims et al., 2002), a fast-spreading ridge with a full spreading rate of 110 mm yr^{-1}. A single Atlantic
100 sample originates from the southern Mid-Atlantic Ridge at ~26° S (Batiza et al., 1988; Niu and Batiza,
101 1994), where the full spreading rate is about 35-40 mm yr^{-1}. We analysed four samples from the
102 Southwest Indian Ridge (SWIR) at 57° E and 66° E (Robinson et al., 1996), which are slow-spreading
103 segments with a full spreading rate of 13-16 mm yr^{-1}. Samples are from neo-volcanic zones with
104 eruption ages <100 ka. None of these sites show any influence of hotspot activity.
105 We focussed on depleted MORB to be representative of the depleted, upper mantle complementary
106 to continental crust. All samples have chondrite normalised La/Sm<1 (Table 1), except one E-MORB

from the Pacific (PH108-1) and two Atlantic E-MORB that represent re-analyses of samples presented in Liang et al. (2017). The radiogenic isotope compositions of our MORB samples are shown in Figure 1, illustrating their generally depleted character (our Pacific and Atlantic MORB have $^{143}Nd/^{144}Nd$ >0.5131) and the distinctive 'DUPAL' signature of SWIR samples, with relatively unradiogenic Pb and Nd and radiogenic Sr.

3 Methods

3.1 Sample preparation

Using a binocular microscope, we hand-picked up to 1.5 g of optically clear glass, without phenocrysts or other inclusions, and carefully avoided visible signs of alteration. Some samples analysed for Mo in this work had already been processed in the U isotope study of Andersen et al. (2015). For these samples, picked glass chips were leached thrice by shaking them for 15 minutes each time in a mixture of 0.05M hydroxylamine hydrochloride, 15% acetic acid and 0.03M EDTA at a pH of 4. This reductive leaching technique (Gutjahr et al., 2007) dissolves Fe-Mn precipitates, such as those that accumulate on sea-floor basalts. These Fe-Mn coatings are potentially problematic, as their strong sorption of elements such as U and Mo from seawater produces a contaminant with contrasting isotopic composition to mantle derived basalts. Consequently, reductive leaching has been widely used in U-series analyses of MORB and this represents an appropriate precautionary step for Mo isotope analysis. For example, inadvertent inclusion of a 10^{-4} mass fraction of Fe-Mn coating with a highly fractionated $\delta^{98/95}$Mo of up to -2‰ in a typical MORB glass analysis would decrease its $\delta^{98/95}$Mo by ~0.07‰.

The leachates were analysed for their elemental contents using an inductively-coupled plasma mass spectrometer (ICP-MS; Thermo Scientific Element 2) at the University of Bristol. As discussed in Andersen et al. (2015), leaching appears to result in minor glass dissolution and so some Mo is removed in the process (see Table S1 in the online Supplementary Materials). Dissolution was most significant in the sample picked from the finest glass fragment size (D14-1). However, there was no systematic, preferential removal during leaching of Mo relative to elements not adsorbed onto Fe-Mn coatings. We therefore inferred our samples were sufficiently young and our picking procedure was sufficiently rigorous that the leaching step was unnecessary, and some of the samples analysed later in the study

were not leached (2370-6, PH108-1, ALV 518-3-2, 45N). Moreover, most samples were analysed for their $^{234}U/^{238}U$ activity ratios, expressed as ($^{234}U/^{238}U$). These activity ratios provide an important check on possible influences of Fe-Mn coatings, which would perturb this ratio from a secular equilibrium value of unity. To check that leaching did not cause any Mo isotope fractionation by preferential dissolution, we analysed a glassed sample of USGS reference material BHVO-2 that then underwent the same leaching procedure (see Andersen et al., 2015 and Table S1). The Mo isotope composition of leached BHVO-2 glass, just like the original powder (Table 1), falls within the reproducibility of BHVO-2 found in the literature (Table S2).

3.2 Analytical techniques

Samples were dissolved in mixtures of high purity 28M HF, 15M HNO_3 and 6M $HClO_4$ after addition of a ^{97}Mo-^{100}Mo double spike and in most cases also a ^{233}U-^{236}U double spike, for high precision $^{238}U/^{235}U$ analysis. Both Mo and U isotope analyses were performed on a Thermo Finnigan Neptune multi-collector ICP-MS (s/n 1020) at the University of Bristol. Pacific samples 2370-6, PH108-1 and a repeat digestion of sample 2504-1 were only spiked with ^{97}Mo-^{100}Mo and analysed for their Mo isotope composition. After digestion and drying, all samples were refluxed twice in 6M HCl to break down fluorides prior to dissolution for ion exchange chromatography. Samples containing a U double spike were first passed through U chemistry protocols. Matrix eluted during U purification was collected, dried and refluxed in 6M HCl for Mo chemistry protocols.

All procedures are described in detail for U in Andersen et al. (2015) and for Mo in Willbold et al. (2016), Hin et al. (2019) and Chen et al. (2019), and we refer the reader to the online Supplementary Material for a brief summary. An important detail is that we monitor both masses 99 and 101 during all measurements and only accept data where Ru interference corrections using both masses yield results within uncertainty of each other (see Supplementary Material). Occasionally, interferences occur on these masses that are evidently not Ru and can influence results without this precaution. Such effects might account for some of the inconsistencies in the current literature, as typically only mass 99 is monitored.

During the course of this study we have analysed $\delta^{98/95}$Mo in a variety of geological reference materials with Mo contents between ~30 ng g^{-1} and ~4 μg g^{-1} and obtained good agreement with literature data (see Table S2). We note that geological reference material W-2a provides a useful test of chemical procedures at low Mo concentrations appropriate for MORB analyses, without the more severe challenge posed by the extremely Mo depleted BIR-1. Based on W-2a analyses in Bristol, presented here and in Chen et al. (2019), the reproducibility of our Mo analyses is ±0.04‰ (2 standard deviations, 2s) as derived from 30 measurements of 16 W-2a digestions; in this study, each of these 30 measurements typically consisted of 3 repeated analyses.

As the number of analyses performed on basalts in this study is ≤3, all uncertainties we present on $\delta^{98/95}$Mo of these individual samples are 2s, based on the long-term reproducibility of W-2a (Table 1). Instead, $\delta^{98/95}$Mo of experimental samples and calculated population means for ocean basins and bulk mantle are presented with 95% confidence intervals (95% c.i.), calculated based on the reproducibility of W-2a for individual samples or based on within-group variance for population means as $t_{0.95} \times s/\sqrt{n}$ where $t_{0.95}$ is a two-way Student's *t*-factor.

Run products of experiments (see below) were analysed by electron microprobe to determine their major and minor element compositions. These analyses were performed on a Jeol JXA8600 at the Department of Archaeology at the University of Oxford, according to the protocols described in Kiseeva and Wood (2013). Both phases were analysed with a 10 μm diameter beam of 20 nA at an accelerating voltage of 15 kV. Values in Table 2 represent means of at least 25 spots, with uncertainties based on the variance of those spots.

3.3 Isotope Fractionation Experiments

We determined experimentally the Mo isotope fractionation between liquid sulphide and liquid silicate to enable accurate predictions of the effects of sulphide extraction during MORB formation and differentiation. Two experiments were performed following the procedures of Kiseeva and Wood (2013). The experimental charges consisted of a 1:1 mixture (by mass) of silicate and FeS powders (see Table 2 for its composition). The silicate powder consisted of a mixture of CaO, MgO, Al_2O_3 and SiO_2

189 in proportions akin to the anorthite-diopside-forsterite eutectic at 1.5 GPa ($An_{50}Di_{28}Fo_{22}$), which is a
190 simplified haplobasalt. This powder was prepared from analytical grade oxides and $CaCO_3$ that were
191 ground and mixed prior to gradual heating from 500°C to 950°C in air and subsequent decarbonation
192 at 950°C for two hours. An additional 10 wt% FeO and 2 wt% MoO_2 powder was then admixed.
193 Samples were loaded into graphite capsules which maintain the oxygen fugacity at or below the C-CO_2-
194 CO equilibrium (1-2 log units below the fayalite-magnetite-quartz buffer). The two experiments were
195 performed in an end-loaded, Boyd-and-England-type piston cylinder apparatus at the University of
196 Oxford at a pressure of 1.5 GPa and a temperature of 1400°C. As Hin et al. (2013) found that Mo
197 isotopes attained equilibrium within 1.5 h between liquid metal and liquid silicate at the same
198 temperature, we ran our two experiments for two and three hours before quenching by cutting the power.
199 More experimental details can be found in Kiseeva and Wood (2013).
200
201 **4 Results**
202 Molybdenum concentrations of our Pacific and Atlantic depleted MORB vary between 0.16 and
203 0.40 μg g^{-1} (Table 1), while our Indian Ocean depleted MORB have markedly higher Mo contents (0.39-
204 0.60 μg g^{-1}) in keeping with the lower degrees of melting at this slow spreading ridge (Robinson et al.,
205 2001). Our Pacific enriched MORB sample (PH108-1) has the highest Mo content of 0.99 μg g^{-1}. Our
206 samples have Ce/Mo between 26 and 55, comparable to MORB reported in other studies that presented
207 isotope dilution measurements of Mo concentrations (Bezard et al., 2016; Liang et al., 2017; Chen et
208 al. 2022).
209 The Mo isotope compositions of our depleted MORB samples vary between −0.16±0.04‰ and
210 −0.27±0.04‰ (Table 1, Figure 2). None of these values are super-chondritic, and 5 of 9 lie outside
211 uncertainties below the chondritic reference. Likewise, mean $\delta^{98/95}$Mo for depleted MORB from
212 different ocean basins have resolved, sub-chondritic values with −0.22±0.04‰ and −0.19±0.03‰ (95%
213 c.i.) for four Pacific and four Indian Ocean samples, respectively. The $\delta^{98/95}$Mo of MORB from Pacific
214 and Indian basins are not statistically distinguishable as different populations ($p_{t\text{-}test}$ 0.40). A single,
215 depleted Atlantic MORB yields −0.27±0.04‰. Overall, we obtain a mean Mo isotope composition of
216 −0.22±0.03‰ (95% c.i.) for our global suite of depleted MORB, i.e. $(La/Sm)_N<1$, which is significantly

below the mean chondritic value of −0.15±0.01‰ (95% c.i.) (Burkhardt et al., 2014; Liang et al., 2017). Our analyses of two enriched Atlantic samples, previously analysed by Liang et al. (2017), yielded $\delta^{98/95}$Mo of −0.04±0.04‰ and −0.06±0.04‰, significantly higher than our depleted MORB.

We report some new (^{234}U/^{238}U) in Table 1, to supplement values previously reported in Andersen et al. (2015). All measurements are within uncertainty (<±0.005) of unity.

Both experiments equilibrating sulphide liquid with silicate liquid show reproducible $\delta^{98/95}$Mo in the quenched glasses as well as in the quenched FeS (Figure 3a and Table 1). We thus obtain an average $\Delta^{98/95}Mo_{sulphide\text{-}silicate}$ of −0.25±0.01‰, i.e. sulphides are 0.25‰ lighter (in terms of ^{98}Mo/^{95}Mo) at 1400°C. We calculated a $\delta^{98/95}$Mo of 0.04±0.01‰ for the bulk run products, based on the mean silicate and sulphide Mo isotope compositions, Mo concentrations and their phase proportions (determined from least squares linear regression of their major element compositions reported in Table 2). This is reassuringly within uncertainty of the value 0.02±0.02‰ determined for the MoO_2 powder used as the starting material. Furthermore, our experiments yielded a sulphide/silicate partition coefficient for Mo of 23.

5 Discussion

5.1 Assessing secondary perturbation of Mo isotope ratios

The primary Mo isotope composition of MORB can be perturbed by direct or indirect interaction with isotopically heavy seawater. Careful picking of fresh glass is the principal means to avoid the former, but it is hard to guard against possible magmatic assimilation of altered crust *en route* to the surface or be sure there are no traces of Fe-Mn coating in picked samples. Based on measurements in drill cores and ocean floor surveys presented in the literature, Hein et al. (2003) estimated that the ocean floor is currently covered by ~2×10^{14} kg of Fe-Mn crust. As this is 7-8 orders of magnitude less than the mass of the magmatic ocean crust, Fe-Mn crusts are irrelevant for its average Mo isotope composition, but as indicated in section 3.1 they can significantly affect $\delta^{98/95}$Mo of individual samples. Reductive leaching acts against such contamination by Fe-Mn crusts, but analysis of (^{234}U/^{238}U) provides an important check for any style of contamination. Pristine MORB display (^{234}U/^{238}U) in secular equilibrium, i.e. with a value of 1. Fe-Mn crusts precipitated from seawater acquire a seawater

245 ($^{234}U/^{238}U$) of about 1.14 (Koide and Goldberg, 1965), and fractionated, isotopically light Mo (Siebert
246 et al., 2003). Portions of mafic crust that have been altered by interaction with seawater inherit both its
247 elevated ($^{234}U/^{238}U$) and isotopically heavy Mo in the process (Freymuth et al., 2015). Critically, all our
248 samples have ($^{234}U/^{238}U$) within error of secular equilibrium. Several of our MORB samples with
249 ($^{234}U/^{238}U$) measured to the highest precision are clearly resolved from a mixing curve to a Fe-Mn
250 contaminant and cannot have acquired their sub-chondritic Mo from such perturbation (Figure 4).
251
252 *5.2 Mo isotope fractionation during magmatic processes*
253 It is important to consider isotopic fractionation during magma genesis when using the isotopic
254 composition of MORB to infer that of the upper mantle. McCoy-West et al. (2019) have recently
255 explored the possibility that Mo isotopes are fractionated during mantle melting, using a model that
256 combines theoretical estimates of fractionation with partitioning and speciation data from petrological
257 experiments. Although a minor species at the current oxygen fugacity of the mantle, Mo^{4+} is isotopically
258 lighter than the dominant Mo^{6+} species and more strongly partitioned into mineral phases, such as
259 pyroxenes (Leitzke et al., 2017). As a net result, the Mo isotope compositions of melts become
260 isotopically heavier than their sources (McCoy-West et al., 2019); MORB, constituting some 10%
261 melting, should have a $\delta^{98/95}$Mo ~0.02‰ higher than the upper mantle from which it is derived, at
262 modern mantle oxygen fugacity. Bezard et al. (2016) previously argued against melt-induced Mo
263 isotope fractionation, based on a lack of systematic variation of $\delta^{98/95}$Mo with degree of melting in their
264 sample set. However, the predicted variability in $\delta^{98/95}$Mo (<0.005‰) due to different degrees of melting
265 in their sample suite is likely too subtle to discern within natural and analytical scatter (e.g. Figure 2),
266 even if all MORB Mo isotope compositions should be systematically slightly heavier than their mantle
267 sources. Furthermore, the effects on Mo isotope ratios of the minor amounts of crystallisation
268 experienced by MORB are likely negligible given the incompatibility of Mo in silicates typically
269 crystallising from MORB.
270 Another potential source of Mo isotope fractionation during magmatic processes is the presence of
271 a sulphide phase (Liang et al., 2017; Voegelin et al., 2014). Chalcophile Mo partitions into sulphide that
272 may be present in the source during melting or that may segregate from MORB during melting and

differentiation, because MORB are frequently sulphide-saturated (Mathez, 1976). Experiments have shown that the partitioning of Mo between liquid sulphide and liquid silicate is strongly dependent on S excess relative to Fe in the sulphide, but sulphide/silicate partition coefficients of Mo during MORB evolution are thought to be likely not much above ~20 (Lodders and Palme, 1991).

Figure 3b presents a Rayleigh distillation model of the effects of sulphide extraction on silicate melt $\delta^{98/95}$Mo, based on the fractionation factor determined in this study. These calculations imply that removal of plausible amounts of immiscible sulphide liquid during melting or differentiation beneath ridges does not significantly affect the $\delta^{98/95}$Mo of the remaining MORB, despite our observation that silicate liquid is enriched in heavy Mo isotopes compared to coexisting sulphide liquid by 0.25±0.01‰ at 1400°C (Figure 3a, Table 1). In these models, we have used an upper limit of 23 for the Mo partition coefficient based on our Ni- and Cu-free experiments. We find that ≥0.5% of the initial mass of the basaltic melt must segregate as sulphide for a measurable isotopic effect of ≥0.04‰ (Figure 3b). Such a mass fraction of sulphide is substantially larger than possible based on S abundances of ~0.2 wt% expected after melting 10% of a peridotite and a minimum S solubility in MORB of ~0.08 wt%, suggesting <0.15% sulphide extraction from MORB (Mathez, 1976). As such we consider the role of sulphide fractionation to have a negligible effect on the $\delta^{98/95}$Mo of MORB relative to its source. Moreover, sulphide removal could only serve to increase the $\delta^{98/95}$Mo of the erupted melt relative to source and cannot explain a melt with sub-chondritic $\delta^{98/95}$Mo derived from a chondritic mantle.

5.3 Sub-chondritic $\delta^{98/95}$Mo of the upper mantle

Although our dataset clearly argues for sub-chondritic $\delta^{98/95}$Mo in depleted portions of the upper mantle, it is important to assess the $\delta^{98/95}$Mo of the upper mantle as a whole. Notably this requires assessing an appropriate global contribution of enriched MORB to the ridge system, as these magmas appear to have higher $\delta^{98/95}$Mo (Bezard et al., 2016; Chen et al., 2022). Trying to appropriately weight contributions of enriched, i.e. $(La/Sm)_N>1$, and depleted MORB, i.e. $(La/Sm)_N<1$, we have used the compilation of Gale et al. (2013) to determine the fraction of global Mo derived from enriched and depleted ridge segments. This exercise shows that for normal ridge segments (i.e. that lie >500 km from

300 a hotspot and are not in a back-arc setting; Gale et al., 2013), 78% of Mo is associated with depleted
301 MORB compositions.

302 We have also calculated concentration-weighted mean $\delta^{98/95}$Mo for depleted and enriched MORB
303 using a compilation of our own and literature data. This requires some care given inconsistencies within
304 published data noted in the introduction and a possible analytical cause of this highlighted in section
305 3.2. We have used data from this study, Chen et al. (2022) and Bezard et al. (2016; excluding their two
306 anomalous, super-chondritic values of depleted MORB from further consideration, as the authors did
307 themselves). We do not include any data from Liang et al. (2017). Their two depleted MORB samples
308 are aberrantly super-chondritic. Although we can replicate their lowest $\delta^{98/95}$Mo (−0.05‰ for enriched
309 MORB ALV 518 3-2), in keeping with McCoy-West et al. (2019), we obtain a lower value for 45N
310 (−0.09‰ vs 0.04‰) and all the other enriched samples of Liang et al (2017) have markedly higher
311 $\delta^{98/95}$Mo than enriched MORB reported by Bezard et al. (2016) or Chen et al. (2022) (Figure 2). From
312 the resulting mean depleted and enriched MORB $\delta^{98/95}$Mo (Table 1) and weighted by the proportion of
313 Mo derived from depleted and enriched ridge segments, we obtain a global mean $\delta^{98/95}$Mo of
314 −0.18±0.01‰ for the melts of the upper mantle. While we recognise that the still limited Mo isotope
315 database makes such a value provisional, it is formally resolved from the chondritic reference. Given
316 the effects of melting (section 5.2), the $\delta^{98/95}$Mo of the upper mantle itself is ~0.02‰ lower than this
317 average MORB value, i.e. −0.20±0.01‰.

318 Previous studies have examined the $\delta^{98/95}$Mo of the Archaean mantle from analyses of komatiites
319 (Greber et al., 2015 and McCoy-West et al., 2019). This dataset is highly variable and further spans to
320 Ce/Mo considerably higher and lower than values of modern, unaltered magmas derived from the
321 mantle (Figure 5). These observations are unsurprising as all komatiites are to some extent altered and
322 metamorphosed and Mo is a fluid mobile element during both processes. Filtering for perturbation,
323 using Mn/Fe^{2+} and Al/Fe^{2+} but not Ce/Mo, McCoy-West et al. (2019) identified nine less altered
324 komatiites, none of which have $\delta^{98/95}$Mo outside uncertainty of the chondritic value (see samples in
325 circles in Figure 5). The mean for these komatiites is statistically sub-chondritic only by considering a
326 standard error of the mean of these samples, but these komatiites are quite unrelated to one another and
327 do not obviously form part of the same population, not least given their variable $^{142}Nd/^{144}Nd$ (Caro and

Bourdon, 2010; Debaille et al., 2013) and $^{182}W/^{184}W$ anomalies (Puchtel et al., 2018; Touboul et al., 2012). We think that the significance of the McCoy-West et al. (2019) mean Mo isotope composition for the Archaean mantle should therefore be treated with caution, particularly at the precision cited. In contrast to the modern case explored above, where 19 out 42 depleted MORB have significantly sub-chondritic $\delta^{98/95}$Mo, only one out of 28 komatiites is resolvably sub-chondritic and this one sample did not pass the filter for weathering employed in McCoy-West et al. (2019).

5.4 Mechanisms for lowering the Mo isotope composition in Earth's mantle

The existence of mantle domains with $\delta^{98/95}$Mo lower than chondrites is geologically relevant because experimental studies imply that equilibrium fractionation during core formation cannot enrich the mantle in light Mo isotopes (Hin et al., 2019, 2013). A putative Hadean sulphide matte of ~0.2 wt% of the mantle (O'Neill, 1991) would not have significantly affected the Mo isotope composition of a post-core formation mantle (see Figure 3b for sulphide extraction effects), which Hin et al. (2019) estimated to be 0.01±0.02‰ heavier than the $\delta^{98/95}$Mo of −0.15±0.01‰ for the bulk Earth. A different process must thus have occurred that lowered a post-core formation $\delta^{98/95}$Mo from an estimated −0.14±0.02‰ to an estimated −0.20±0.01‰ in Earth's modern mantle.

5.4.1 Isotopically light Mo in melted residual mantle

McCoy-West et al. (2019) argued that melting very likely results in Mo isotope fractionation. Although no experiments have yet been performed to confirm these theoretical calculations, empirical support for this idea may be found in the work of Chen et al. (2022). This study accounted for correlations of $\delta^{98/95}$Mo with $(La/Sm)_N$ in MORB and seamount lavas as the result of Mo isotope fractionation by small degree (<2%) melting of depleted mantle. Chen et al. (2022) argued that such small degree melts migrated into the oceanic mantle lithosphere, were recycled with it and remained isolated sufficiently long (~1 Ga) to further evolve radiogenic isotopic signatures appropriate for enriched MORB. The magnitude of Mo isotope fractionations required by this model are consistent with those predicted by McCoy-West et al. (2019).

A corollary of isotopically heavy Mo in melts is that the residue becomes isotopically light. At high degrees of melting, such as for MORB, the majority of an incompatible element such as Mo will be concentrated in the melt. By mass balance, high degree melts must closely represent the initial mantle composition and the Mo depleted residue is perturbed to lighter $\delta^{98/95}$Mo than its starting composition. In this way, McCoy-West et al. (2019) argued that the sub-chondritic $\delta^{98/95}$Mo they inferred for Archaean mantle resulted as a complement to early, continental crust formation. From a simple Mo isotope mass-balance, they inferred an Archaean proto-continental crust at least as large as the current continental volume to account for the sub-chondritic $\delta^{98/95}$Mo in Archaean mantle.

As discussed in section 5.3, we believe it is premature to characterise the $\delta^{98/95}$Mo of the Archaean mantle as sub-chondritic using the current komatiite dataset. Nonetheless, the modern, depleted mantle may still reflect the consequences of magmatic Mo fractionation during the extraction of the continental crust. There are two important problems with such a model. As noted by McCoy-West et al. (2019), it is difficult to reproduce the best estimate for modern continental crust ($\delta^{98/95}$Mo ~0.1‰; Yang et al., 2017) in simple melting scenarios. Given its incompatibility, most mantle melts are enriched in Mo and by mass balance their $\delta^{98/95}$Mo must lie close to their initial, unmelted mantle value, so it is the depleted residual mantle that becomes isotopically light rather than the melt complement becoming significantly heavier in its Mo isotope signature. McCoy-West et al. (2019) acknowledged this problem and argued for repeated remelting of the crust to increase continental $\delta^{98/95}$Mo. To have a net effect on continental composition, however, a substantial fraction of Mo needs to be accommodated into mafic cumulates that are delaminated back to the mantle.

A potentially more important consideration is that the modern, depleted mantle has several distinctive trace element ratios, e.g. high U/Th, Nb/U, Ce/Pb that are complementary to the modern continental crust, but cannot be a result of simple magmatic processes, during which the elements in these ratios show similar incompatibility (e.g. Hofmann, 1988). Element fractionations associated with plate recycling and subduction zone processes are widely believed to be responsible for these key trace element signatures (Hofmann, 1988; Miller et al., 1994). It therefore makes sense to examine if isotopic fractionation of Mo might be a consequence of the same subduction zone processes.

383 *5.4.2 Subduction zone fractionation of Mo isotopes*

384 A growing number of studies show that arc lavas have isotopically heavy Mo isotopic
385 compositions. Some argue for a role in fractionation of hydrous phases in generating such elevated
386 $\delta^{98/95}$Mo (Gaschnig et al., 2017; Voegelin et al., 2014; Wille et al., 2018), but mafic arc lavas, which
387 can have experienced minimal fractionation of Mo isotopes due to differentiation, commonly have
388 markedly higher $\delta^{98/95}$Mo than MORB (Freymuth et al., 2015; König et al., 2016; Li et al., 2021;
389 Villalobos-Orchard et al., 2020), with an average of ~0.03‰. Such lavas are also characterised by low
390 Ce/Mo due to the relative mobility of Mo in fluids, as well as by low Ce/Pb and Nb/U. Therefore, arc
391 lavas have both $\delta^{98/95}$Mo much closer to the values of continental crust than simple mantle melts and
392 further carry key complementary trace element signatures to balance mantle depletion.

393 A consequence of isotopically heavy Mo in arc lavas is that the subduction-processed residue must
394 be isotopically light. This has been clearly documented by Chen et al. (2019), who studied Mo isotope
395 compositions in exhumed, MORB-like eclogites and found that they have $\delta^{98/95}$Mo as low as −0.7‰,
396 accompanied by higher Ce/Mo than MORB. The authors showed this process is driven by retention of
397 isotopically light Mo in rutile and they argued that the isotopically heavy Mo was lost to the arc by
398 transportation in dehydration fluids. They modelled this quantitatively using an experimentally
399 determined Mo isotope fractionation factor between rutile and hydrous melt. The fluxing of the
400 subducting slab with fluids also depletes the slab in fluid mobile Pb (Miller et al., 1994) but results in a
401 relative enrichment in Nb, that strongly partitions into rutile, creating an ocean crust residue with low
402 $\delta^{98/95}$Mo and high Nb/U and Ce/Pb ratio. Recycling of this fluid-fluxed, residual crust back into the
403 mantle can account for the key chemical features we wish to explain.

404 We undertake quantitative assessment of this process in the next section but here briefly clarify
405 our conceptual model. We consider an overall depleted mantle (e.g. $(La/Sm)_N<1$) complementary to an
406 ancient continental crust. Since the onset of plate tectonics, the continual formation and destruction of
407 oceanic plates makes this reservoir heterogenous, with harzburgitic and basaltic components recycled
408 back into this depleted mantle. The former component dominates volumetrically but the latter is the
409 chief repository of incompatible elements. Although the recycled ocean crust is more enriched than the
410 averaged mantle from which it is derived, we argue that the recycled mafic crust is not the source of

411 enriched MORB, contrary to some studies (Prinzhofer et al., 1989; Yang et al., 2020). The important
412 feature we highlight is that enriched MORB is characterised by isotopically heavy Mo (Bezard et al.,
413 2016; Chen et al., 2022), whereas recycled mafic crust is isotopically light (Chen et al., 2019). This
414 observation makes recycled mafic crust an unlikely contributor to enriched MORB. Instead, we invoke
415 enriched MORB is generated by addition of a third component in the oceanic lithosphere, i.e. portions
416 of the harzburgitic lithosphere that have been metasomatized by small degree melts frozen into its base.

417 All recycled lithosphere will comprise comparable proportions of harzburgite and basaltic crust,
418 but the distribution of melts frozen into the base of the lithosphere is likely governed by local upwelling
419 and is not ubiquitous. The three components of recycled lithosphere will become intimately juxtaposed
420 by convective stirring (Allègre and Turcotte, 1986) together with mantle residual to continental
421 extraction that has not yet been processed through the ridge system. We note that the main incompatible
422 element contributors to typical MORB are the recycled, basaltic crust and residual mantle. A full
423 compositional range from depleted to enriched MORB further requires variable contributions of melts
424 from the harzburgitic mantle lithosphere and its metasomatized portions, respectively, that are mixed
425 within an erupted batch of MORB. Due to the extreme incompatible element depletion of the
426 harzburgitic lithosphere, variability in this component is best fingerprinted using the least incompatible
427 Lu-Hf isotopic system (Salters et al., 2011). We argue that the 'all normal MORB' average of Gale et
428 al. (2013) represents the globally averaged melt contributions from the four different lithologies. Our
429 model simply tracks the long-term evolution of this averaged, depleted, reservoir and does not attempt
430 to reproduce any detail created by source heterogeneity.

431 Key to our arguments is the recycling of mafic crust. The modification of this crust during
432 subduction leads to net evolution of the mantle, by loss of fluid mobile elements to the continents. In
433 major element terms, however, the mantle is at near steady state as subduction resupplies a fusable,
434 basaltic component to the mantle to allow continued melting over Ga timescales. The recycled mafic
435 crust is an intrinsic part of this dynamic, but overall depleted mantle, such that the trace element
436 compositions imposed on the recycled crust by subduction become integral to the depleted MORB
437 source.

438

439 *5.4.3 Model of molybdenum cycling*

440 In this section we calculate the influence of recycling subduction-processed mafic crust on the
441 $\delta^{98/95}$Mo evolution of the mantle using a simple mass balance model. We also examine the related
442 evolution of Ce/Pb. We chose Ce/Pb rather than other distinct incompatible element ratios of the
443 modern, depleted mantle, such as Nb/U or Th/U, that have also been argued to result from plate cycling,
444 as Ce/Pb is most closely linked to $\delta^{98/95}$Mo, via loss of Pb and Mo during fluid fluxing of the mafic
445 crust. The role of recycling in influencing U budgets is dominantly a result of seafloor alteration and so
446 not as easily tied to Mo isotope fractionation in the subduction zone. A quantitative discussion of Ce/Mo
447 in the mantle with time is complicated by the poorly constrained Ce/Mo in the early Earth, which needs
448 to be estimated by accounting for the siderophile behaviour of Mo.

449 The model extracts a mass flux of Mo, Ce and Pb during subduction dehydration over time and
450 stores this flux in the continental crust. We calculate these mass fluxes from modern estimates of global
451 arc production rates, arc length and element contents of arc lavas, and subtract them from the mantle to
452 determine its evolving concentrations of Mo, Ce and Pb. All details are described in the Supplementary
453 Information, including the option to investigate the effect of sediment fluxes to mimic continental crust
454 recycling, but the general form of the equations is given here with the example of the Mo isotope
455 evolution of the mantle:

456 $$\delta Mo_{dm,t_i} = \frac{M_m C^{Mo}_{dm,t_{i-1}} \delta Mo_{dm,t_{i-1}} - (t_i - t_{i-1}) flux^{Mo}_{arc,t_i} \delta Mo_{dm,t_{i-1}}}{M_m C^{Mo}_{dm,t_{i-1}} - (t_i - t_{i-1}) flux^{Mo}_{arc,t_i}} \quad (1)$$

457 where M_m is the mass of the mantle, C^{Mo}_{dm} the Mo concentration in the modelled mantle, t_i is time
458 at time-step i, and $flux^{Mo}_{arc}$ the flux of Mo mass extracted from the mantle at arcs. This example uses
459 data on arc lava compositions to calculate element fluxes, but we also used the contrasting Mo contents
460 and isotopic compositions of MORB and exhumed, MORB-like eclogites to estimate the flux extracted
461 from the mantle over time for the Mo isotope system. Although results for Mo isotope ratios are similar
462 using this alternative approach, it is less suitable for Ce/Pb because this ratio is typically disturbed in
463 eclogites due to late-stage fluid migration (see Supplementary Information for more model details).

464 Figure 6 shows that the modelled mantle gradually obtains a lighter Mo isotope composition as
465 mixing subduction residues with low $\delta^{98/95}$Mo into the mantle progresses with time, following

466 preferential removal of heavy Mo isotopes during slab dehydration. It is poorly constrained what
467 proportions of subducting oceanic crust are recycled in the upper mantle or reach the lower mantle.
468 Additionally, the mantle is chemically heterogeneous, implying that chemical mixing is not perfect. In
469 our recycling model, we circumvented these complexities by modelling two end-member scenarios of
470 perfect chemical mixing in either the whole mantle or the upper mantle, the upper mantle referring to
471 the mass of the mantle above the seismic discontinuity at 660 km depth. We compare these model
472 results to the mean $\delta^{98/95}$Mo of −0.20±0.01‰ we determined in section 5.3 for the upper mantle.
473 If all subducting oceanic crust is recycled into the upper mantle (red lines in Figure 6), ~1.1 Gyr
474 of subduction lowers the $\delta^{98/95}$Mo to a value of −0.20‰, while simultaneously increasing Ce/Pb to the
475 value of ~30 estimated for the upper mantle (Workman and Hart, 2005). If all subducted oceanic crust
476 is homogenised into the whole mantle, this timescale increases to ~3.9 Gyr (black lines in Figure 6).
477 Recycling 10% of a subducting sediment layer of globally averaged thickness into the upper mantle
478 (Figure 6, broken, red curve) slightly increases the model timescales to ~1.4 Gyr for both $\delta^{98/95}$Mo and
479 Ce/Pb. This sediment fraction is equivalent to 0.5% of sediment in the recycled oceanic crust, which
480 falls within the range of 0-2.2% sediment in the mixtures of recycled crust and depleted mantle modelled
481 by Chauvel et al. (2008) that successfully reproduced the Hf-Nd isotope array of MORB. The timescales
482 considered for the upper mantle scenario are within recent estimates for the duration of modern plate
483 tectonics (e.g. Dhuime et al., 2012) and the great oxidation event. Prior to that time the compositions of
484 modern arc lavas and eclogites we used to estimate chemical fractionation during slab dehydration may
485 not be applicable due to changing redox conditions in subduction zones. The longer timescales in the
486 whole mantle recycling scenario appear to require an additional process to aid in lowering the mantle's
487 $\delta^{98/95}$Mo and increasing its Ce/Pb, or alternatively imply that mixing is not uniform throughout the whole
488 mantle. Nonetheless, our simple attempt at quantifying the influence of subducting oceanic crust on the
489 composition of Earth's depleted mantle implies that this process can simultaneously account for the
490 high Ce/Pb and low $\delta^{98/95}$Mo observed in many depleted MORB. Mo isotope fractionation during partial
491 melting could aid in lowering $\delta^{98/95}$Mo of the residual mantle, but not in substantially increasing its
492 Ce/Pb (Figure 6).
493

6 Conclusions

We document that depleted MORB commonly have resolvably sub-chondritic Mo isotope compositions. For the upper mantle as a whole, we estimate $\delta^{98/95}$Mo = −0.20±0.01‰, which is also sub-chondritic. Prior work has established that core formation cannot account for a sub-chondritic mantle $\delta^{98/95}$Mo. We argue against melt fractionation of Mo isotopes as the dominant cause for low $\delta^{98/95}$Mo in the upper mantle (McCoy-West et al., 2019), as this process does not readily account for associated, diagnostic trace element fractionations (e.g. Ce/Pb) nor current estimates of the $\delta^{98/95}$Mo of continental crust. We propose that subduction-processed mafic crust, which previous work has shown to have isotopically light Mo (Chen et al., 2019) and high Ce/Pb (Miller et al., 1994), remixed back into the upper mantle can better account for current observations. In a simple model we quantitatively show that such a process can impart the requisite chemical signatures over a few billion yeas of plate tectonic cycling. Notwithstanding its chemical heterogeneity, our work implies that the ambient mantle most commonly sourced during MORB melting is a mixture of mantle complementary to an ancient continental crust and subducted ocean crust.

Acknowledgements

We thank Chris Coath for indispensable help with the mass spectrometer and Carolyn Taylor for her contributions to sample preparations. Insightful reviews by Andreas Stracke and an anonymous reviewer greatly helped to improve our manuscript, while we appreciated Fred Moynier's fair and quick editorial handling. Kevin Burton kindly provided splits of samples 45N and ALV 518-3-2. We acknowledge support from NERC grants NE/L007428/1 and NE/H023933/1 as well as from NERC studentship NE/I528250/1 to Kate Hibbert.

References

Allègre, C.J., Turcotte, D.L., 1986. Implications of a two-component marble-cake mantle. Nature 323, 123–127. https://doi.org/10.1038/323123a0

Andersen, M.B., Elliott, T., Freymuth, H., Sims, K.W.W., Niu, Y.L., Kelley, K.A., 2015. The

terrestrial uranium isotope cycle. Nature 517, 356-U463. https://doi.org/10.1038/nature14062

Batiza, R., Melson, W.G., Ohearn, T., 1988. Simple Magma Supply Geometry Inferred beneath a Segment of the Mid-Atlantic Ridge. Nature 335, 428–431.

Bezard, R., Fischer-Godde, M., Hamelin, C., Brennecka, G.A., Kleine, T., 2016. The effects of magmatic processes and crustal recycling on the molybdenum stable isotopic composition of Mid-Ocean Ridge Basalts. Earth Planet. Sci. Lett. 453, 171–181.

Burkhardt, C., Hin, R.C., Kleine, T., Bourdon, B., 2014. Evidence for Mo isotope fractionation in the solar nebula and during planetary differentiation. Earth Planet. Sci. Lett. 391, 201–211. https://doi.org/10.1016/j.epsl.2014.01.037

Caro, G., Bourdon, B., 2010. Non-chondritic Sm/Nd ratio in the terrestrial planets: Consequences for the geochemical evolution of the mantle crust system. Geochim. Cosmochim. Acta 74, 3333–3349.

Chauvel, C., Lewin, E., Carpentier, M., Arndt, N.T., Marini, J.C., 2008. Role of recycled oceanic basalt and sediment in generating the Hf-Nd mantle array. Nat. Geosci. 1, 64–67. https://doi.org/10.1038/ngeo.2007.51

Chen, S., Hin, R.C., John, T., Brooker, R., Bryan, B., Niu, Y., Elliott, T., 2019. Molybdenum systematics of subducted crust record reactive fluid flow from underlying slab serpentine dehydration. Nat. Commun. https://doi.org/10.1038/s41467-019-12696-3

Chen, S., Sun, P., Niu, Y., Guo, P., Elliott, T., Hin, R.C., 2022. Molybdenum isotope systematics of lavas from the East Pacific Rise : Constraints on the source of enriched mid-ocean ridge basalt. Earth Planet. Sci. Lett. 117283. https://doi.org/10.1016/j.epsl.2021.117283

Debaille, V., O'Neill, C., Brandon, A.D., Haenecour, P., Yin, Q.Z., Mattielli, N., Treiman, A.H., 2013. Stagnant-lid tectonics in early Earth revealed by Nd-142 variations in late Archean rocks. Earth Planet. Sci. Lett. 373, 83–92. https://doi.org/10.1016/j.epsl.2013.04.016

Dhuime, B., Hawkesworth, C.J., Cawood, P.A., Storey, C.D., 2012. A change in the geodynamics of

546 continental growth 3 billion years ago. Science (80-.). 335, 1334–1336.
547 https://doi.org/10.1126/science.1216066

548 Freymuth, H., Vils, F., Willbold, M., Taylor, R.N., Elliott, T., 2015. Molybdenum mobility and
549 isotopic fractionation during subduction at the Mariana arc. Earth Planet. Sci. Lett. 432, 176–
550 186.

551 Gale, A., Dalton, C.A., Langmuir, C.H., Su, Y., Schilling, J.G., 2013. The mean composition of ocean
552 ridge basalts. Geochemistry, Geophys. Geosystems. https://doi.org/10.1029/2012GC004334

553 Gaschnig, R.M., Reinhard, C.T., Planavsky, N.J., Wang, X.L., Asael, D., Chauvel, C., 2017. The
554 Molybdenum Isotope System as a Tracer of Slab Input in Subduction Zones: An Example From
555 Martinique, Lesser Antilles Arc. Geochemistry Geophys. Geosystems 18, 4674–4689.
556 https://doi.org/10.1002/2017gc007085

557 Greber, N.D., Puchtel, I.S., Nagler, T.F., Mezger, K., 2015. Komatiites constrain molybdenum isotope
558 composition of the Earth's mantle. Earth Planet. Sci. Lett. 421, 129–138.
559 https://doi.org/10.1016/j.epsl.2015.03.051

560 Gutjahr, M., Frank, M., Stirling, C.H., Klemm, V., van de Flierdt, T., Halliday, A.N., 2007. Reliable
561 extraction of a deepwater trace metal isotope signal from Fe-Mn oxyhydroxide coatings of
562 marine sediments. Chem. Geol. 242, 351–370.

563 Hein, J.R., Koschinsky, A., Halliday, A.N., 2003. Global occurrence of tellurium-rich ferromanganese
564 crusts and a model for the enrichment of tellurium. Geochim. Cosmochim. Acta 67, 1117–1127.
565 https://doi.org/10.1016/S0016-7037(00)01279-6

566 Henderson, G.M., Burton, K.W., 1999. Using (234U/238U) to assess diffusion rates of isotope tracers
567 in ferromanganese crusts. Earth Planet. Sci. Lett. 170, 169–179. https://doi.org/10.1016/S0012-
568 821X(99)00104-1

569 Hin, R.C., Burkhardt, C., Schmidt, M.W., Bourdon, B., Kleine, T., 2013. Experimental evidence for
570 Mo isotope fractionation between metal and silicate liquids. Earth Planet. Sci. Lett. 379, 38–48.

https://doi.org/DOI 10.1016/j.epsl.2013.08.003

Hin, R.C., Burnham, A.D., Gianolio, D., Walter, M.J., Elliott, T., 2019. Molybdenum isotope fractionation between Mo4+ and Mo6+ in silicate liquid and metallic Mo. Chem. Geol. 504, 177–189. https://doi.org/10.1016/j.chemgeo.2018.11.014

Hofmann, A.W., 1988. Chemical Differentiation of the Earth - the Relationship between Mantle, Continental-Crust, and Oceanic-Crust. Earth Planet. Sci. Lett. 90, 297–314.

Kiseeva, E.S., Wood, B.J., 2013. A simple model for chalcophile element partitioning between sulphide and silicate liquids with geochemical applications. Earth Planet. Sci. Lett. 383, 68–81. https://doi.org/10.1016/j.epsl.2013.09.034

Koide, M., Goldberg, E.D., 1965. Uranium-234/uranium-238 ratios in sea water. Prog. Oceanogr. 3, 173–177. https://doi.org/10.1016/0079-6611(65)90016-9

König, S., Wille, M., Voegelin, A., Schoenberg, R., 2016. Molybdenum isotope systematics in subduction zones. Earth Planet. Sci. Lett. 447, 95–102. https://doi.org/10.1016/j.epsl.2016.04.033

Leitzke, F.P., Fonseca, R.O.C., Sprung, P., Mallmann, G., Lagos, M., Michely, L.T., Münker, C., 2017. Redox dependent behaviour of molybdenum during magmatic processes in the terrestrial and lunar mantle: Implications for the Mo/W of the bulk silicate Moon. Earth Planet. Sci. Lett. 474, 503–515.

Li, H.Y., Zhao, R.P., Li, J., Tamura, Y., Spencer, C., Stern, R.J., Ryan, J.G., Xu, Y.G., 2021. Molybdenum isotopes unmask slab dehydration and melting beneath the Mariana arc. Nat. Commun. 12, 1–10. https://doi.org/10.1038/s41467-021-26322-8

Liang, Y.H., Halliday, A.N., Siebert, C., Fitton, J.G., Burton, K.W., Wang, K.L., Harvey, J., 2017. Molybdenum isotope fractionation in the mantle. Geochim. Cosmochim. Acta 199, 91–111. https://doi.org/10.1016/j.gca.2016.11.023

Lodders, K., Palme, H., 1991. On the Chalcophile Character of Molybdenum - Determination of

596 Sulfide Silicate Partition-Coefficients of Mo and W. Earth Planet. Sci. Lett. 103, 311–324.
597 https://doi.org/Doi 10.1016/0012-821x(91)90169-I

598 Mathez, E.A., 1976. Sulfur solubility and magmatic sulfides in submarine basalt glass. J. Geophys.
599 Res. 81, 4269–4276. https://doi.org/10.1029/JB081i023p04269

600 McCoy-West, A.J., Chowdhury, P., Burton, K.W., Sossi, P., Nowell, G.M., Fitton, J.G., Kerr, A.C.,
601 Cawood, P.A., Williams, H.M., 2019. Extensive crustal extraction in Earth's early history
602 inferred from molybdenum isotopes. Nat. Geosci. 12, 946–953.

603 Miller, D.M., Goldstein, S.L., Langmuir, C.H., 1994. Cerium/lead and lead isotope ratios in arc
604 magmas and the enrichment of lead in the continents. Nature. https://doi.org/10.1038/368514a0

605 Niu, Y.L., Batiza, R., 1994. Magmatic processes at a slow-spreading ridge segment - 26°S Mid-
606 Atlantic Ridge. J. Geophys. Res. Earth 99, 19719–19740. https://doi.org/10.1029/94jb01663

607 Niu, Y.L., Collerson, K.D., Batiza, R., Wendt, J.I., Regelous, M., 1999. Origin of enriched-type mid-
608 ocean ridge basalt at ridges far from mantle plumes: The East Pacific Rise at 11 degrees 20 ' N.
609 J. Geophys. Res. Earth 104, 7067–7087.

610 O'Neill, H.S.C., 1991. The origin of the Moon and the early history of the Earth - a chemical model.
611 Part 2. The Earth. Geochim. Cosmochim. Acta 55, 1159–1172. https://doi.org/10.1016/0016-
612 7037(91)90169-6

613 Prinzhofer, A., Lewin, E., Allègre, C.J., 1989. Stochastic melting of the marble cake mantle: evidence
614 from local study of the East Pacific Rise at 12°50′N. Earth Planet. Sci. Lett. 92, 189–206.
615 https://doi.org/10.1016/0012-821X(89)90046-0

616 Puchtel, I.S., Blichert-Toft, J., Touboul, M., Walker, R.J., 2018. 182W and HSE constraints from 2.7
617 Ga komatiites on the heterogeneous nature of the Archean mantle. Geochim. Cosmochim. Acta
618 228, 1–26. https://doi.org/10.1016/j.gca.2018.02.030

619 Regelous, M., Niu, Y.L., Wendt, J.I., Batiza, R., Greig, A., Collerson, K.D., 1999. Variations in the
620 geochemistry of magmatism on the East Pacific Rise at 10 degrees 30 ' N since 800 ka. Earth

621 Planet. Sci. Lett. 168, 45–63.

622 Robinson, C.J., Bickle, M.J., Minshull, T.A., White, R.S., Nichols, A.R.L., 2001. Low degree melting
623 under the Southwest Indian Ridge: The roles of mantle temperature, conductive cooling and wet
624 melting. Earth Planet. Sci. Lett. 188, 383–398. https://doi.org/10.1016/S0012-821X(01)00329-6

625 Robinson, C.J., White, R.S., Bickle, M.J., Minshull, T.A., 1996. Restricted melting under the very
626 slow-spreading Southwest Indian ridge. Geol. Soc. London, Spec. Publ. 118, 131–141.
627 https://doi.org/10.1144/GSL.SP.1996.118.01.07

628 Salters, V.J.M., Mallick, S., Hart, S.R., Langmuir, C.E., Stracke, A., 2011. Domains of depleted
629 mantle: New evidence from hafnium and neodymium isotopes. Geochemistry Geophys.
630 Geosystems 12, 1–18. https://doi.org/10.1029/2011GC003617

631 Siebert, C., Nagler, T.F., von Blanckenburg, F., Kramers, J.D., 2003. Molybdenum isotope records as
632 a potential new proxy for paleoceanography. Earth Planet. Sci. Lett. 211, 159–171.

633 Sims, K.W.W., Goldstein, S.J., Blichert-Toft, J., Perfit, M.R., Kelemen, P., Fornari, D.J., Michael, P.,
634 Murrell, M.T., Hart, S.R., DePaolo, D.J., Layne, G., Ball, L., Jull, M., Bender, J., 2002.
635 Chemical and isotopic constraints on the generation and transport of magma beneath the East
636 Pacific Rise. Geochim. Cosmochim. Acta 66, 3481–3504. https://doi.org/10.1016/S0016-
637 7037(02)00909-2

638 Touboul, M., Puchtel, I.S., Walker, R.J., 2012. 182W evidence for long-term preservation of early
639 mantle differentiation products. Science (80-.). 335, 1065–1069.
640 https://doi.org/10.1126/science.1216351

641 Villalobos-Orchard, J., Freymuth, H., O'Driscoll, B., Elliott, T., Williams, H., Casalini, M., Willbold,
642 M., 2020. Molybdenum isotope ratios in Izu arc basalts: The control of subduction zone fluids
643 on compositional variations in arc volcanic systems. Geochim. Cosmochim. Acta 288, 68–82.
644 https://doi.org/10.1016/j.gca.2020.07.043

645 Voegelin, A.R., Pettke, T., Greber, N.D., von Niederhausern, B., Nagler, T.F., 2014. Magma

differentiation fractionates Mo isotope ratios: Evidence from the Kos Plateau Tuff (Aegean Arc). Lithos 190, 440–448. https://doi.org/10.1016/j.lithos.2013.12.016

Willbold, M., Hibbert, K., Lai, Y.J., Freymuth, H., Hin, R.C., Coath, C., Vils, F., Elliott, T., 2016. High-Precision Mass-Dependent Molybdenum Isotope Variations in Magmatic Rocks Determined by Double-Spike MC-ICP-MS. Geostand. Geoanalytical Res. 40, 389–403. https://doi.org/10.1111/j.1751-908X.2015.00388.x

Wille, M., Nebel, O., Pettke, T., Vroon, P.Z., Konig, S., Schoenberg, R., 2018. Molybdenum isotope variations in calc-alkaline lavas from the Banda arc, Indonesia: Assessing the effect of crystal fractionation in creating isotopically heavy continental crust. Chem. Geol. 485, 1–13. https://doi.org/10.1016/j.chemgeo.2018.02.037

Workman, R.K., Hart, S.R., 2005. Major and trace element composition of the depleted MORB mantle (DMM). Earth Planet. Sci. Lett. 231, 53–72. https://doi.org/10.1016/j.epsl.2004.12.005

Yang, J., Barling, J., Siebert, C., Fietzke, J., Stephens, E., Halliday, A.N., 2017. The molybdenum isotopic compositions of I-, S- and A-type granitic suites. Geochim. Cosmochim. Acta 205, 168–186. https://doi.org/10.1016/j.gca.2017.01.027

Yang, S., Humayun, M., Salters, V.J.M., 2020. Elemental constraints on the amount of recycled crust in the generation of mid-oceanic ridge basalts (MORBs). Sci. Adv. 6, 1–13. https://doi.org/10.1126/sciadv.aba2923

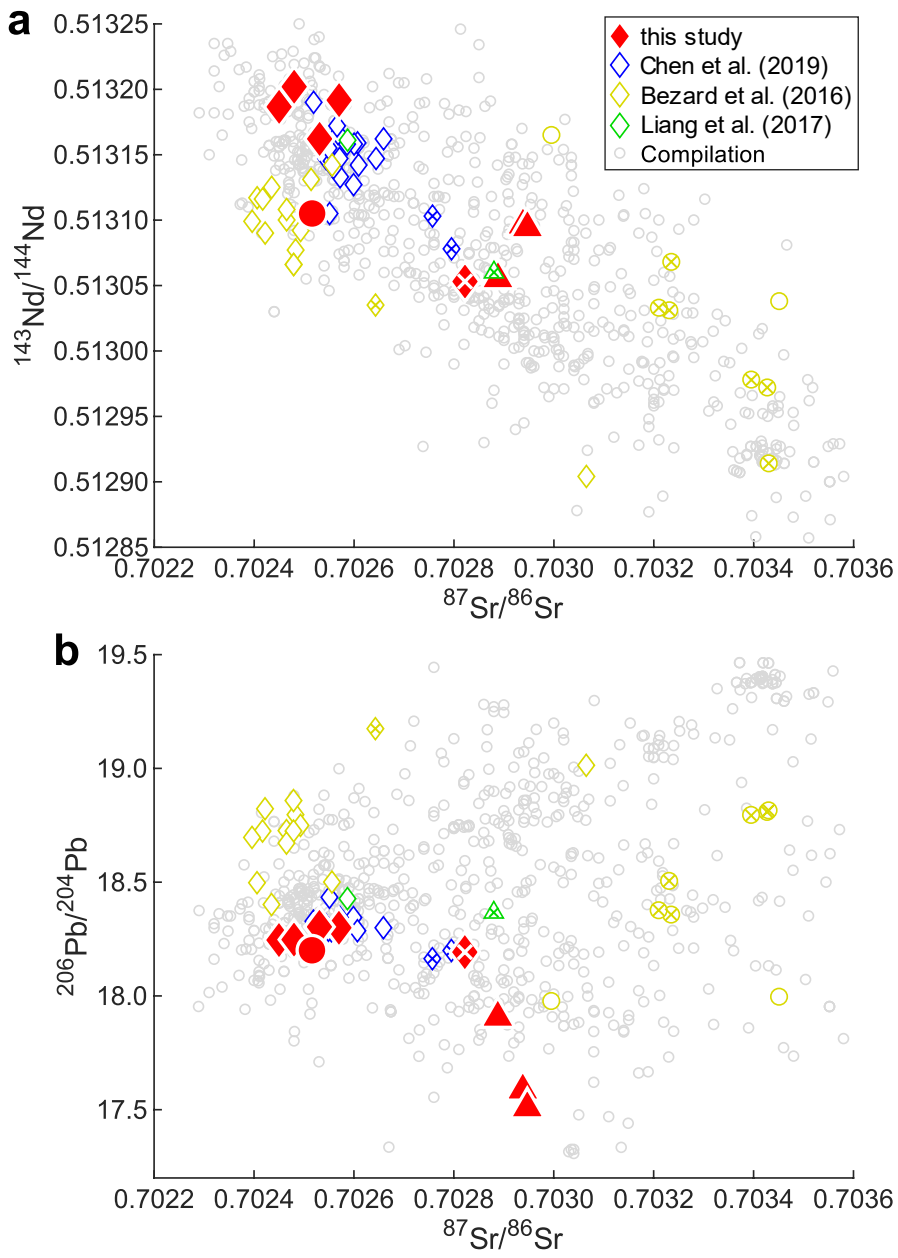

Figure 1. Radiogenic isotope compositions of mid-ocean ridge basalts (MORB) studied for $\delta^{98/95}Mo_{NIST\ SRM\ 3134}$. a) $^{143}Nd/^{144}Nd$ against $^{87}Sr/^{86}Sr$, b) $^{206}Pb/^{204}Pb$ against $^{87}Sr/^{86}Sr$. Samples from the Pacific Ocean are depicted as diamonds, the Atlantic Ocean as circles and the Indian Ocean as triangles. Symbols with a cross represent enriched MORB with $(La/Sm)_N>1$. Compilation of mid-ocean ridge basalt data from PETDB repository based on a search for volcanic basalts from spreading centres. Note that a few of these repository data plot outside the scale of both panels. Note that depleted Indian MORB have a DUPAL-like signature typical of MORB from this ocean basin.

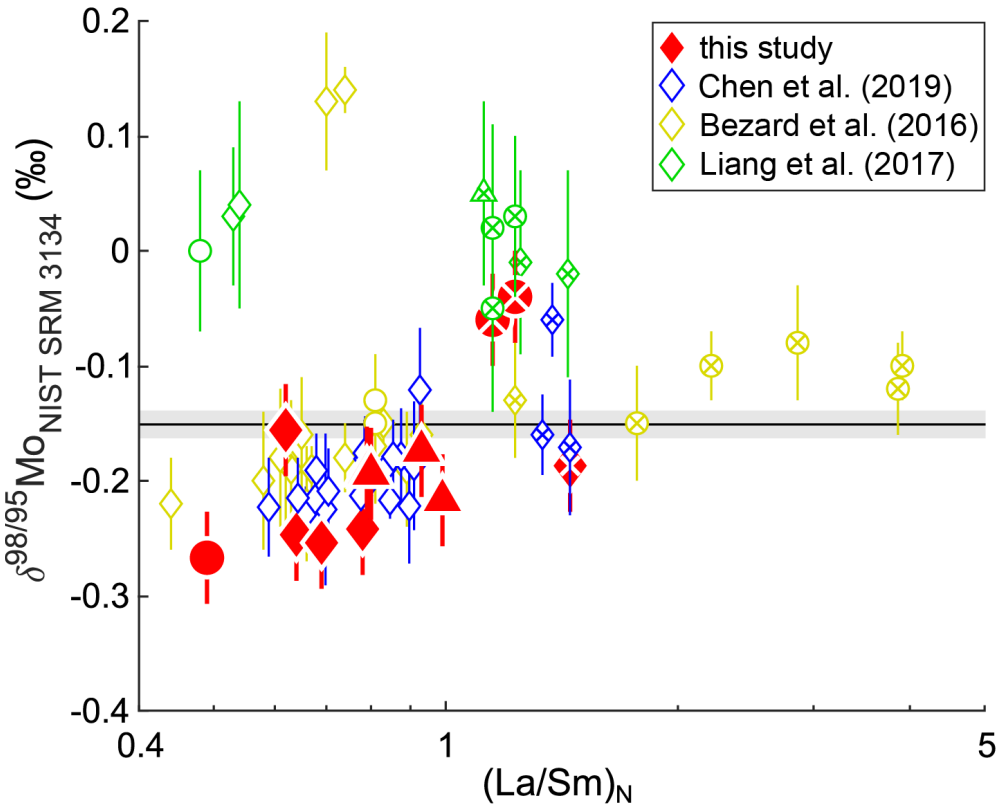

Figure 2. Mo isotope compositions of mid-ocean ridge basalts against their chondrite-normalised La/Sm. Samples from the Pacific Ocean are depicted as diamonds, the Atlantic Ocean as circles and the Indian Ocean as triangles. Symbols with a cross represent enriched MORB. Note that three depleted MORB of Liang et al. (2017) and two of Bezard et al. (2016) with anomalously high $\delta^{98/95}$Mo are excluded from further discussion in our present study (see main text for further discussion). The mean $\delta^{98/95}Mo_{NIST\ SRM\ 3134}$ estimated for the bulk Earth is shown by the black line, with the grey field representing its 95% confidence interval (Burkhardt et al., 2014; Liang et al., 2017).

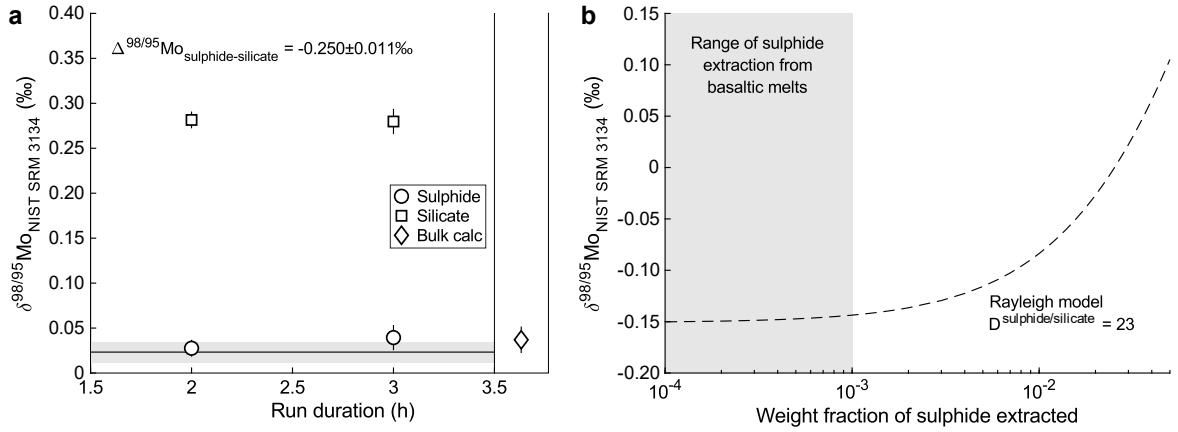

Figure 3. a) Mo isotope compositions observed in experiments that equilibrated silicate liquid with sulphide liquid at 1.5 GPa and 1400°C, plotted as a function of experimental run duration. The black line and shaded rectangle depict the measured $\delta^{98/95}Mo_{NIST\ SRM\ 3134}$ and its uncertainty in MoO_2 powder used in the starting mixture. b) Modelled Mo isotope evolution of residual silicate liquid as a function of sulphide extraction following Rayleigh fractionation. The initial $\delta^{98/95}Mo_{NIST\ SRM\ 3134}$ of −0.15‰ in the modelled silicate liquid is based on the estimated Mo isotope composition of the bulk Earth. The modelling was performed assuming an equilibration temperature of 1200°C between sulphide and silicate liquids using a Mo isotope fractionation factor of –0.32‰, adapted from our experimentally determined fractionation factor assuming proportionality to the square of temperature. We used a value of 23 for the sulphide/silicate partition coefficient of Mo, based on the experiments we performed for this study.

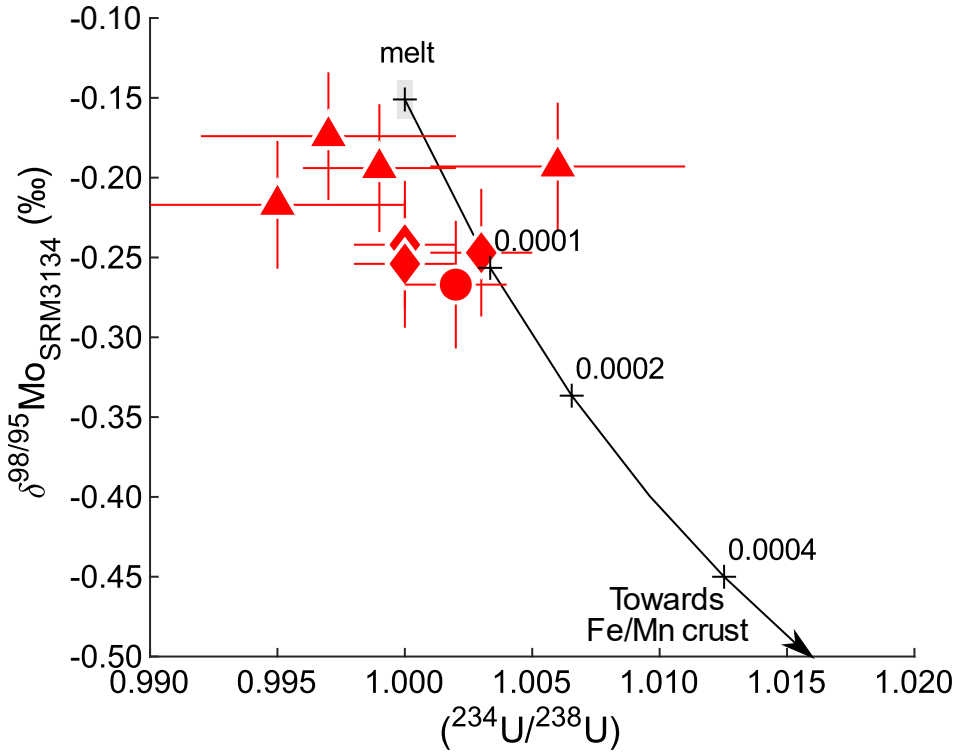

Figure 4. Mo isotope compositions of mid-ocean ridge basalts from this study plotted against their ($^{234}U/^{238}U$). Arrow illustrates effect of mixing between an uncontaminated melt and Fe-Mn crust. "Plus" marks and values along the arrowed mixing line indicate mass fraction of Fe-Mn crust in the mixture. Note that several samples are resolved from the mixing line, indicating that their sub-chondritic Mo isotope composition cannot be explained by contamination with Fe-Mn crust. Composition of the melt used in the mixing calculation: $\delta^{98/95}Mo_{SRM3134} = -0.15‰$, estimated bulk Earth composition based on the mean of representative chondrites and iron meteorites in Burkhardt et al., 2014, and Liang et al., 2017; Mo content = 0.3 μg g^{-1}, based on mean for MORB in this study; ($^{234}U/^{238}U$) = 1; and U content = 0.055 μg g^{-1}, based on the mean for D-MORB in Gale et al., 2003. Composition used for Fe-Mn crusts: $\delta^{98/95}Mo_{SRM3134} = -0.92‰$ and Mo content = 477 μg g^{-1} (Siebert et al., 2003); ($^{234}U/^{238}U$) = 1.144 and U content = 13.1 μg g^{-1} (Henderson and Burton, 1999).

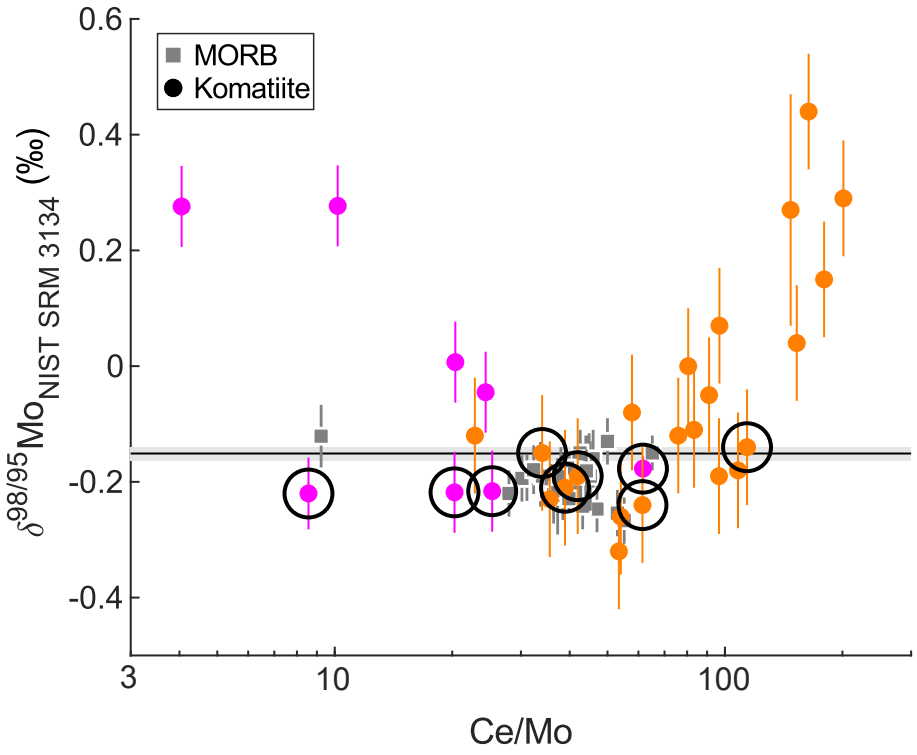

Figure 5. Mo isotope compositions of depleted mid-ocean ridge basalts (grey; this study, Bezard et al., 2016, Chen et al., 2022) and komatiites from Greber et al. (2015; orange) and McCoy-West et al. (2019; magenta), plotted against their Ce/Mo. The estimated $\delta^{98/95}$Mo of the bulk Earth is shown as a black line with the grey field representing its 95% confidence interval. Samples in circles have been used by McCoy-West et al. (2019) to derive a $\delta^{98/95}$Mo in the Archaean mantle, based on filtering the komatiite data set for weathering effects using their Mn/Fe^{2+} and Al/Fe^{2+}. All data have 2s uncertainties. The relatively large uncertainties on the komatiite data are likely due to lower measurement intensities caused by the low Mo contents in komatiites.

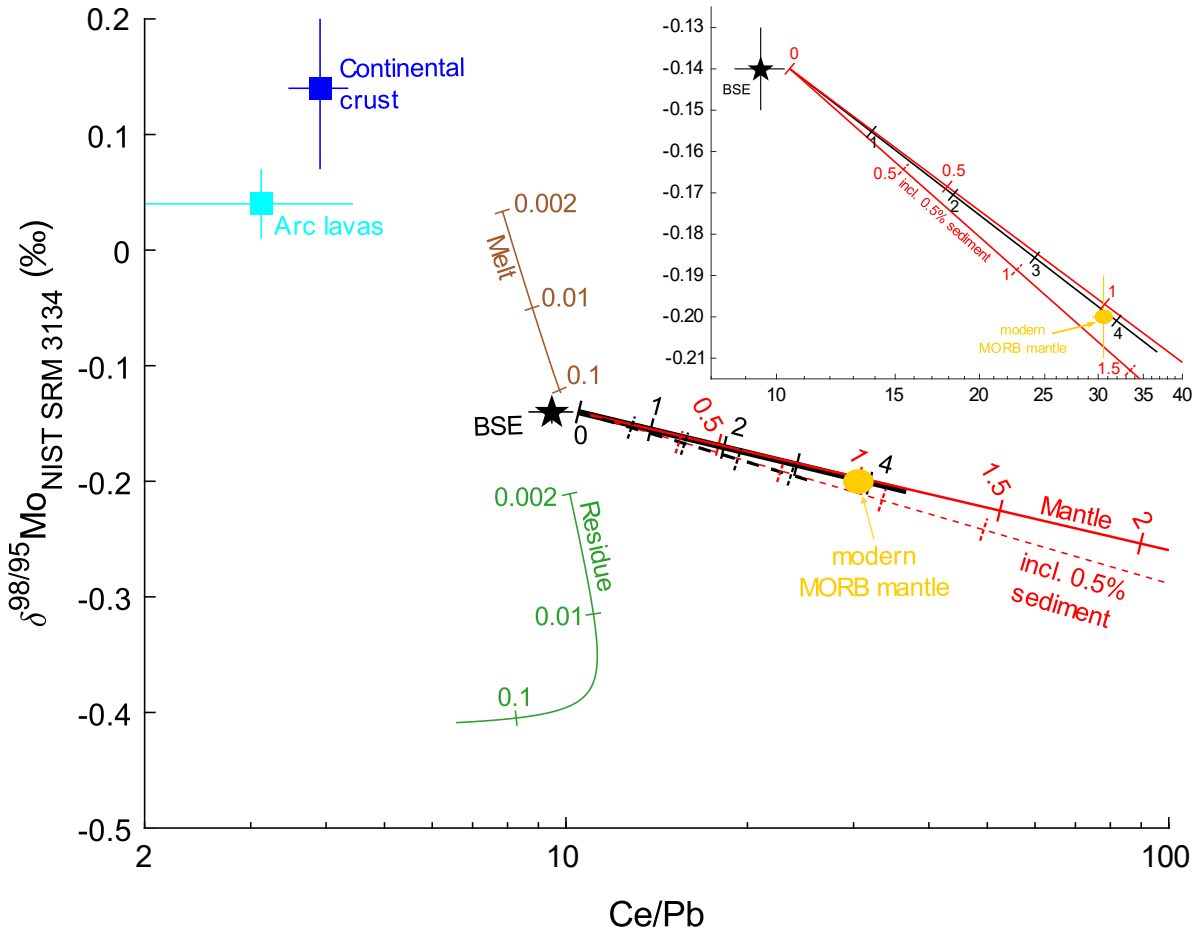

Figure 6. Modelled Mo isotope compositions and Ce/Pb evolution of the mantle. The modelled mantle following oceanic crust subduction into the whole mantle (black line) or into the upper mantle (red line) is shown with tick marks indicating the time of continued subduction in Gyr. Broken lines depict model results in which the subducted slab contains 0.5% (by weight) sediment (see text and Supplementary Information for details). The modelled compositions of melt (brown curve) and residue (green curve) following mantle melting are depicted with melt fractions from 0.2% to ~15% (cpx-out). Subduction lowers the Mo isotope composition of the modelled mantle as processing of oceanic crust in subduction zones enriches the residue in light Mo isotopes and in Ce relative to Pb, storing their complements (similar to arc lavas) in continental crust. This model runs through the estimated composition of the modern (depleted) MORB mantle with $\delta^{98/95}$Mo from our study and Ce/Pb from Workman and Hart (2005). Top-right inset focusses on the results of this model to better display the individual curves (note that to this effect, the curve for the whole mantle including 0.5% sediment recycling is not shown.) As mantle melting barely fractionates Ce/Pb, modelled melt does not approach modern arc lava or continental crust compositions, nor does a modelled melt residue approach the modern MORB mantle composition. Compositions of the various reservoirs are depicted here by their mean with 95% confidence interval on their $\delta^{98/95}$Mo and 1s uncertainty on their Ce/Pb. See Supplementary Information for individual compositions of reservoirs.

Table 1. Results of mid-ocean ridge basalts and and liquid sulphide – liquid silicate experiments. depl. = depleted.

Sample		$(La/Sm)_N$ [1]	Mo (µg/g)	$\delta^{98/95}Mo_{NIST\ SRM\ 3134}$ (‰)	2s 95% c.i. [2]	n	$^{234/238}U$	2se	$^{87/86}Sr$	$^{143/144}Nd$	$^{206/204}Pb$	ref.
Pacific ocean basin												
2504-1			0.193	-0.23	0.04	*1*						
	replicate		0.206	-0.26	0.04	*2*						
	mean	*0.64*	*0.200*	*-0.25*	*0.04*		*1.003*	*0.002*	0.70245	0.513187	18.245	1
2370-6[3]		0.62	0.205	-0.16	0.04	*3*			0.70257	0.513192	18.299	1
2372-1		0.63	0.212	-0.23	0.04	*1*	1.000	0.002	0.70248	0.513202	18.247	2
PH65-1		0.69	0.405	-0.25	0.04	*1*	1.000	0.002	0.702531	0.513162	18.303	3
PH108-1[3]		1.45	0.987	-0.19	0.04	*2*			0.702822	0.513053	18.192	4
	Mean, depl. MORB		*0.247*	*-0.22*	*0.04*	*4*						
Atlantic ocean basin												
D14-1		0.49	0.162	-0.27	0.04	*1*	1.002	0.002	0.702554	0.513107	18.289	5
ALV 518-3-2[3]		1.15	0.216	-0.06	0.04	*1*						6
45N[3]		1.23	0.410	-0.04	0.04	*2*						7
Indian ocean basin												
4/13C		0.79	0.602	-0.19	0.04	*2*	1.006	0.005	0.702938	0.513096	17.585	8
5/15G		0.99	0.390	-0.22	0.04	*2*	0.995	0.005				8
8/26F		0.80	0.556	-0.19	0.04	*3*	0.999	0.003	0.702947	0.513094	17.507	8
12/37F		0.93	0.375	-0.17	0.04	*1*	0.997	0.005	0.702888	0.513055	17.905	8
	Mean, depl. MORB		*0.481*	*-0.19*	*0.03*	*4*						
	Mean, all depl. MORB			***-0.22***	***0.03***	***9***						
	Mean global depl. MORB [3]			***-0.19***	***0.01***	***42***						
	Mean global enr. MORB [4]			***-0.12***	***0.03***	***11***						
Geological reference material												
BHVO-2[5]	powder		4.35	-0.06	0.04	*2*						
BHVO-2	glass		3.49	-0.04	0.04	*1*						
Sulphide-silicate experiments												
sulphide 2h				0.03	0.02	9						
sulphide 3h				0.04	0.03	4						
	mean			*0.03*	*0.01*	13						
silicate 2h				0.28	0.02	9						
silicate 3h				0.28	0.03	4						
	mean			*0.28*	*0.01*	13						
Starting mixture				0.02	0.02	6						

[1]La/Sm normalised to a chondritic La/Sm of 1.57.

[2]Standard deviations based on long-term reproducibility of geological reference material W2a are given for all individual samples of mid-ocean ridge basalt, as their number of repeated analyses are ≤3. Uncertainties for experiments as well as for ocean basin means are 95% confidence intervals calculated as s/sqrt(n)*$t_{0.95}$ where s is the standard deviation based on the relevant samples and $t_{0.95}$ is the value for a two-sided Student t-distribution with 95% confidence region.

[3]Concentration-weighted mean of MORB with $(La/Sm)_N<1$ in this study, Bezard et al. (2016) and Chen et al. (2022), excluding two outliers in Bezard et al. (2016).

[4]Concentration-weighted mean of MORB with $(La/Sm)_N>1$ in this study, Bezard et al. (2016) and Chen et al. (2022).

[5]Samples were not leached.

References for radiogenic isotope ratios and La/Sm: 1 Sims et al. (2002); 2 Sun et al. (2003); 3 Regelous et al. (1999); 4 Niu et al. (1999); 5 Regelous et al. (2009); 6 Gannoun et al. (2007); 7 Schilling et al. (1983), note that they refer to sample 45°N as "Hudson 56-3"; 8 Robinson (1998).

Table 2. Compositions (wt%) of silicate glass and sulphide determined gravimetrically (starting mixture) or by electron microprobe, except for Mo contents in KK29-1 glass and sulphide, which were determined by isotope dilution with a double isotope tracer.

Species	*Starting mixture*	*KK29-1 glass*	*2sd*	*KK29-1 sulphide*	*2sd*
FeS	49.9				
SiO_2	20.1	42.3	0.2		
Al_2O_3	7.92	15.1	0.2		
MgO	7.70	14.4	0.5		
CaO	7.49	16.1	0.4		
FeO	5.43	9.6	0.3		
Na_2O		0.12	0.02		
K_2O		0.006	0.011		
TiO_2		0.014	0.018		
MnO		0.04	0.03		
SO_2		0.56	0.06		
P_2O_5		0.008	0.008		
Mo[1,2]	1.06	0.0546	0.0011		
Fe				61.4	2.2
S				34.1	2.0
O				2.6	1.0
Si				0.00	0.03
Ni				0.02	0.03
Mo[2]				1.25	0.02
W				0.02	0.07
Total		98.2	0.5	99.4	3.2

[1]Mo was added to the starting mixture as MoO_2.

[2]Mo concentrations in KK29-1 glass and sulphide were determined by double-spiked isotope ratio analysis. They have been given an estimated 2% relative uncertainty based on the small sample masses of a few mg.